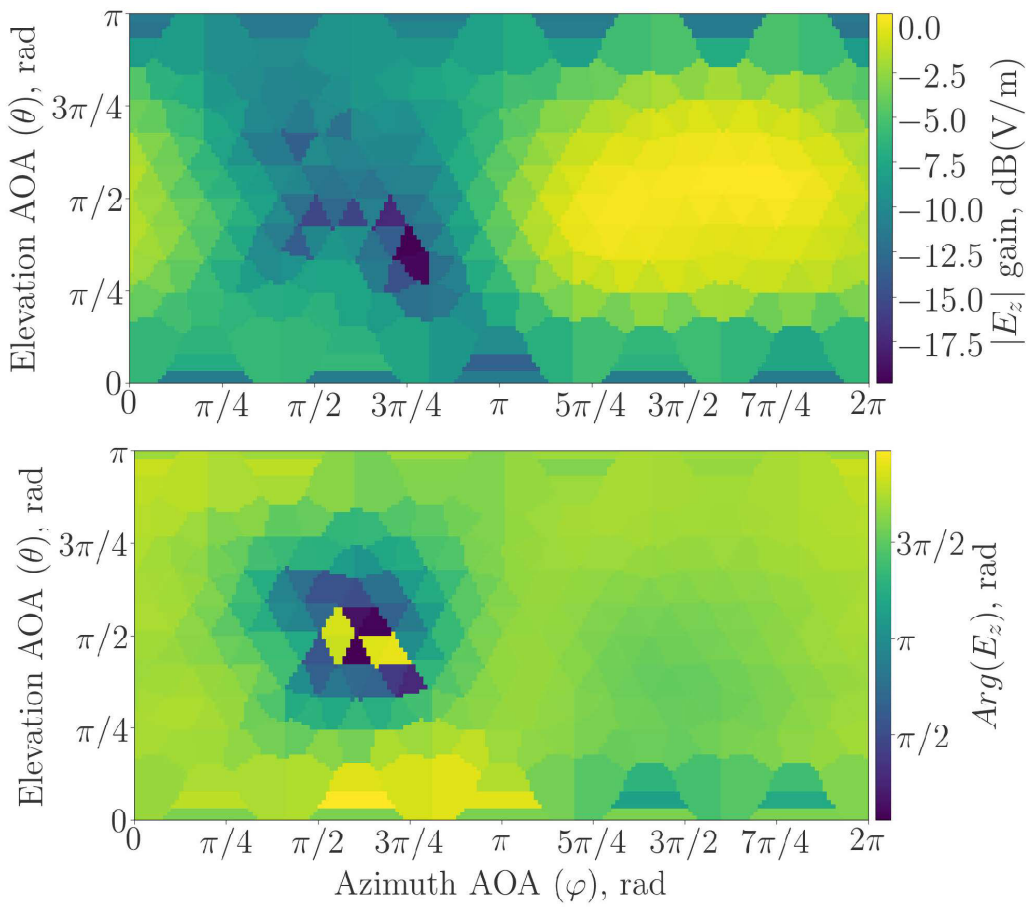

Figure 2. Top: Gain of the vertical polarization component of the E-field for the UE positioned next to the left side of the phantom's head. Bottom: Phase of the vertically polarized E-field as a function of direction of incidence. φ = 3π/2 rad (azimuth) and θ = π/2 rad (elevation) correspond to the direct incidence to the UE, and φ = π/2 correspond to the signal blocked by the head.

S03-4 [17:45] - YOUNG SCIENTIST PAPER

Exposure assessment of body-implanted capsules in the 100-MHz–5-GHz range

Denys Nikolayev[1, 2], Wout Joseph[2], Maxim Zhadobov[3], Ronan Sauleau[3], Luc Martens[2] & Anja Skrivervik[1]

[1]*Microwaves and Antennas Group (MAG), École polytechnique fédérale de Lausanne, Lausanne, Switzerland, CH-1015*

[2]*INTEC – WAVES, imec / Ghent University, Ghent, Belgium, BE-9052*

[3]*Univ Rennes, CNRS, IETR (Institut d'Électronique et de Télécommunications de Rennes) UMR–6164, Rennes, France, FR-35000*

Keywords: Dosimetry (computational), RF/Microwaves, Completed (unpublished)

Presented by: Denys Nikolayev

Body-implanted bioelectronics rely on antennas to interface with external on- or off-body equipment. For a given input power, the antenna type and operating frequency significantly affect the power dissipation in tissues. This study addresses the exposure by realistic magnetic and electric equivalent sources using full-wave modeling techniques. The effect of equivalent source configuration on the power dissipation, exposure,

and radiation performance is here quantified for the first time. The results demonstrate the existence of mode-dependent optimal operating frequency that maximizes the achievable radiation efficiency and minimizes Specific Absorption Rate (SAR) for a given input power.

Introduction

Wirelessly connected body-implanted bioelectronics offers attractive capabilities for clinical research, medicine, defense, and professional sports [1]–[3]. For example, wireless biomedical telemetry enables continuous monitoring of a wide range of human or animal physiological parameters: vitals, blood tests, organ functions monitoring, etc. Precision medicine requires precise diagnostics [4], and miniature body-implanted capsules realize more precise data than ever before about one's health. Neural interfaces allow us to study the brain via mapping, assisting, augmenting, and repairing cognitive or sensory-motor functions [5]. The emerging concept of electroceuticals aims individual neural circuits that regulate the physiological processes to treat a wide range of illnesses [6]. Continuous innovations in micro-electro-mechanical systems (MEMS), integrated circuits, and microfluidics further accelerate the progress in implantable bioelectronics.

In-body bioelectronics commonly use radiofrequency (RF) antennas to communicate with external on- or off-body systems. Establishing a robust link between an in-body device and external equipment is a major challenge because of low radiation efficiencies ($\eta < 0.1\%$) due to significant power dissipation in tissues [7] and miniature size of the radiating elements. A wide range of RF antennas has been proposed for body-implantable applications, e.g. [8]–[15]. In 100-MHz–5-GHz range, the dosimetric quantity used to characterize the in-body exposure levels is SAR [16], ICNIRP, [17]. Whereas the exposure analysis of the realistic body-implanted antennas has been widely reported, there is a lack of systematic knowledge on how the different antenna types and operating frequencies affect the power dissipation. This study addresses this issue by comparing radiation performance and SAR of fundamental finite-sized TM_{10} and TE_{10} equivalent sources in the frequency range from 100 MHz to 5 GHz.

Methods

Exposure of body-implanted capsules is analyzed theoretically using the stratified ∅100-mm spherical phantom [18]. The four-region Cole–Cole model [19] represents dispersive muscle-, fat-, and skin-equivalent electromagnetic (EM) properties of the phantom. The EM field radiated from an arbitrary source in tissues satisfies the inhomogeneous wave equation. In terms of the time-harmonic electric field $\mathbf{E}$ (time variations of the form $e^{j\omega t}$), it is expressed as $\nabla^2\mathbf{E} = j\omega\mu\mathbf{J}_s + j\omega\mu\sigma\mathbf{E} - \omega^2\mu\varepsilon\mathbf{E}$, where $\mathbf{J}_s$ is the source electric current density [20]. Assuming axial symmetry for the formulated problem $\mathbf{E}(r,\varphi,z) = \mathbf{E}(r, z)\exp(-jm\varphi)$, where m is the azimuthal mode number, we reduce the model complexity to $\mathbf{R}^2$.

We consider two realistic equivalent-source formulations: 1) the $\mathbf{E}$-coupled source radiating TM_{10} mode and 2) the magnetic $\mathbf{B}$-coupled (TE_{10}) source. The sources are modeled as $\mathbf{J}_s(r,\varphi,z)$ distribution over a parametrized cylindrical surface enclosed in a capsule volume (Figure 1). The geometrical parameters used in this study are chosen to represent a typical in-body capsule [3] (units: millimeters): the length of the cylindrical part L = 13, its radius R = 4, and shell thickness T = 1 (total volume v = 1.54 cm^3). These parameters result in the overall capsule dimensions 23 × ∅10 mm. The relative permittivity $\varepsilon_{r,S}(f)$ of the capsule volume (Figure 1) equals $\varepsilon_r(f)$ of the surrounding medium (dispersive muscle) whereas the conductivity is zero. It is assumed that the capsule is composed of nonmagnetic materials (i.e. $\mu \equiv \mu_0$). The distribution of $\mathbf{J}_s$ is defined on the cylindrical surface as $\mathbf{J}_{s,TM} = [0, 0, \cos(\pi z/L)]$ A·m^{-2} for the TM_{10} source and as $\mathbf{J}_{s,TE} = [0, 1, 0]$ A·m^{-2} for the TE_{10} one. The supplied P^s, radiated P^r, and dissipated P^d powers are calculated as in [21]. The radiation efficiency η is evaluated using the conservation of energy principle. Local $SAR = \sigma|\mathbf{E}|^2/\rho$ is calculated considering the density of muscle tissue $\rho = 1041$ kg·m^{-3}. The problem is solved with a finite-element method in $\mathbf{R}^2$ using an axisymmetric time-harmonic formulation [22].

Results and Discussion

The results in Figure 2 demonstrate that the optimal radiation performance of a body-implanted capsule requires minimizing the dissipated energy for a given power flow in the far field of the antenna. For an

omnidirectional antenna with given input power, the maximum operating range and data rates can only be improved by increasing the radiation efficiency. The achievable efficiency for both TM_{10} and TE_{10} sources is proportional to the electrical size of the antenna until the power dissipation losses start to dominate at $f > f_{opt}$ (Figure 2), where f_{opt} is the optimal frequency defined as $\eta(f_{opt}) \equiv \max(\eta)$. TM_{10} source allows for higher $\max(\eta)$ compared to TE_{10}. However, TE_{10} provides substantially better efficiency for $f \lessapprox 0.7$ GHz. This is consistent with the fundamental limits on maximum power densities reaching free space [23]. Figure 3 shows the SAR distributions. Both TM_{10} and TE_{10} sources show reduced absorption when the source operates within the optimal frequency range.

Conclusions

This study addressed the lack of systematic knowledge on how the different antenna types and operating frequencies affect the power dissipation. The results revealed the existence of mode-dependent optimal operating frequency that maximizes the achievable radiation efficiency and minimizes SAR for a given input power. Derived values of $\max(\eta)$ indicate that it is possible to outperform state-of-the-art antenna designs up to a factor of five in terms of radiation performance without increasing the input power and SAR.

Acknowledgment

This study was supported in part by the Université Bretagne Loire (UBL), in part by the European Union through the European Regional Development Fund (ERDF), and in part by the French region of Brittany, Ministry of Higher Education and Research, Rennes Métropole and Conseil Départemental 35, through the CPER Project SOPHIE / STIC & Ondes.

References

[1] A. S. Y. Poon, “Miniaturized Biomedical Implantable Devices,” in Implantable Bioelectronics, Weinheim, Germany: Wiley-VCH, 2014, pp. 45–64.

[2] A. Kiourti and K. S. Nikita, “A review of in-body biotelemetry devices: implantables, ingestibles, and injectables,” IEEE Trans. Biomed. Eng., vol. 64, no. 7, pp. 1422–1430, Jul. 2017.

[3] D. Nikolayev, M. Zhadobov, R. Sauleau, and P. Karban, “Antennas for ingestible capsule telemetry,” in Advances in Body-Centric Wireless Communication: Applications and State-of-the-Art, London, UK: IET, 2016, pp. 143–186.

[4] S. J. Aronson and H. L. Rehm, “Building the foundation for genomics in precision medicine,” Nature, vol. 526, no. 7573, pp. 336–342, Oct. 2015.

[5] J. J. Jun et al., “Fully integrated silicon probes for high-density recording of neural activity,” Nature, vol. 551, no. 7679, pp. 232–236, Nov. 2017.

[6] K. Famm, B. Litt, K. J. Tracey, E. S. Boyden, and M. Slaoui, “Drug discovery: A jump-start for electroceuticals,” Nature, vol. 496, pp. 159–161, Apr. 2013.

[7] A. K. Skrivervik, “Implantable antennas: The challenge of efficiency,” in Proc. 7th Eur. Conf. on Antennas and Propagation (EuCAP 2013), Gothenburg, Sweden, 2013, pp. 3627–3631.

[8] S. Bakogianni and S. Koulouridis, “On the design of miniature MedRadio implantable antennas,” IEEE Trans. Antennas Propag., vol. 65, no. 7, pp. 3447–3455, Jul. 2017.

[9] Z. Bao, Y.-X. Guo, and R. Mittra, “Conformal capsule antenna with reconfigurable radiation pattern for robust communications,” IEEE Trans. Antennas Propag., vol. 66, no. 7, pp. 3354–3365, Apr. 2018.

[10] W. Lei and Y. Guo, “Design of a dual-polarized wideband conformal loop antenna for capsule endoscopy systems,” IEEE Trans. Antennas Propag., vol. 66, no. 11, pp. 5706–5715, Nov. 2018.

[11] F. Merli, L. Bolomey, J. Zurcher, G. Corradini, E. Meurville, and A. K. Skrivervik, “Design, realization and measurements of a miniature antenna for implantable wireless communication systems,” IEEE Trans. Antennas Propag., vol. 59, no. 10, pp. 3544–3555, Oct. 2011.

[12] M. S. Miah, A. N. Khan, C. Icheln, K. Haneda, and K. Takizawa, “Antenna system design for improved wireless capsule endoscope links at 433 MHz,” IEEE Trans. Antennas Propag., 2019.

[13] D. Nikolayev, M. Zhadobov, L. Le Coq, P. Karban, and R. Sauleau, “Robust ultra-miniature capsule antenna for ingestible and implantable applications,” IEEE Trans. Antennas Propag., vol. 65, no. 11, pp. 6107–6119, Nov. 2017.

[14] Y. Peng, K. Saito, and K. Ito, “Antenna design for impulse-radio-based wireless capsule endoscope communication systems,” IEEE Trans. Antennas Propag., vol. 66, no. 10, pp. 5031–5042, Oct. 2018.

[15] J. Wang, M. Leach, E. G. Lim, Z. Wang, R. Pei, and Y. Huang, “An implantable and conformal antenna for wireless capsule endoscopy,” IEEE Antenn. Wireless Propag. Lett., vol. 17, no. 7, pp. 1153–1157, Jul. 2018.

[16] IEEE, “IEEE Standard for Safety Levels with Respect to Human Exposure to Radio Frequency Electromagnetic Fields, 3 kHz to 300 GHz,” IEEE, New York, NY, C95.1-2005, 2005.

[17] The International Commission on Non-Ionizing Radiation Protection, “Guidelines for limiting exposure to time-varying electric, magnetic, and electromagnetic fields (up to 300 GHz),” Health Physics, vol. 74, pp. 494–522, 1998.

[18] D. Nikolayev, M. Zhadobov, and R. Sauleau, “Impact of tissue electromagnetic properties on radiation performance of in-body antennas,” IEEE Antenn. Wireless Propag. Lett., vol. 17, no. 8, pp. 1440–1444, Aug. 2018.

[19] S. Gabriel, R. W. Lau, and C. Gabriel, “The dielectric properties of biological tissues: III. Parametric models for the dielectric spectrum of tissues,” Phys. Med. Biol., vol. 41, pp. 2271–2293, Nov. 1996.

[20] J. D. Jackson, Classical electrodynamics, 3rd ed. Hoboken, NJ: John Wiley & Sons, 1999.

[21] D. Nikolayev, M. Zhadobov, P. Karban, and R. Sauleau, “Electromagnetic radiation efficiency of body-implanted devices,” Phys. Rev. Applied, vol. 9, no. 2, p. 024033, Feb. 2018.

[22] P. Karban, F. Mach, P. Kůs, D. Pánek, and I. Doležel, “Numerical solution of coupled problems using code Agros2D,” Computing, vol. 95, no. 1, pp. 381–408, 2013.

[23] A. K. Skrivervik, M. Bosiljevac, and Z. Sipus, “Fundamental limits for implanted antennas: Maximum power density reaching free space,” IEEE Trans. Antennas Propag., in press.

Figures

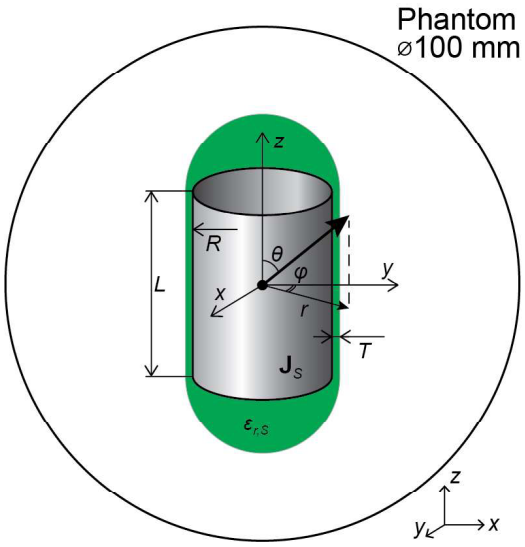

Figure 1. Problem formulation (not to scale).

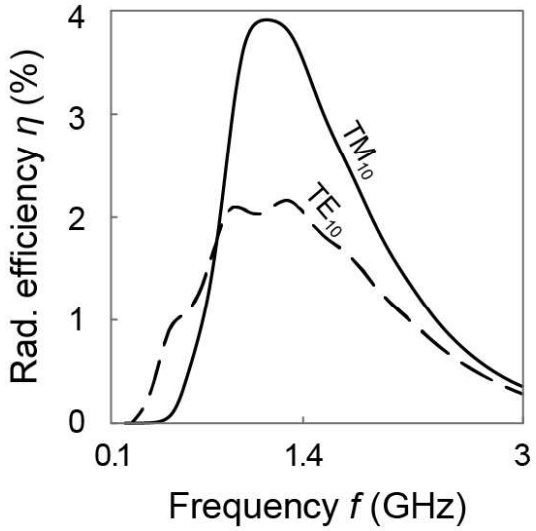

Figure 2. Maximum achievable radiation efficiencies $\eta = 1 - P_d/P_s$ of body-implanted capsules follow skew-normal distribution. The achievable efficiencies of both TM_{10} and TE_{10} sources are proportional to the electrical size of the antenna until the power dissipation losses start to dominate at $f > f_{opt}$

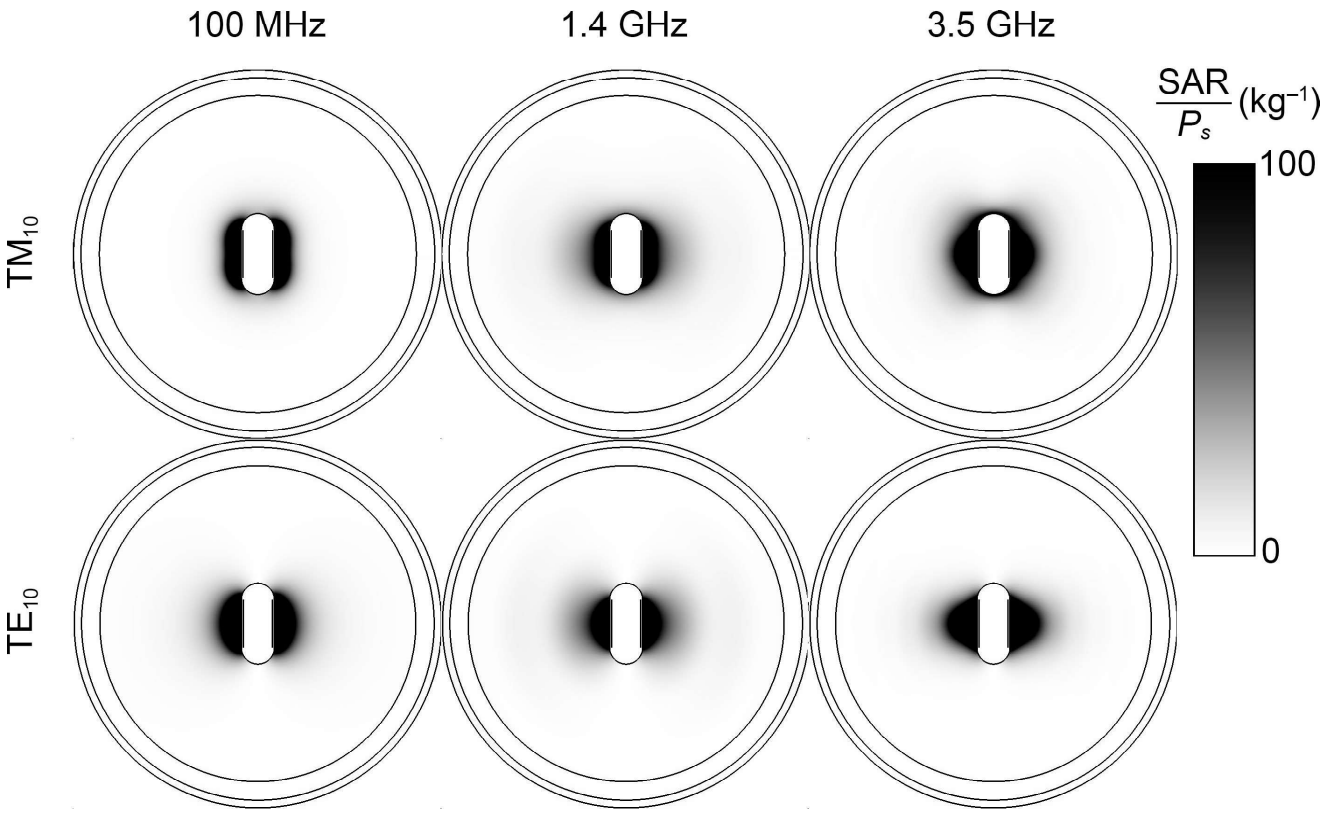

Figure 3. SAR distributions normalized by the supplied power P_s of TM_{10} and TE_{10} sources at 100 MHz (electrically small inefficient source), 1.4 GHz (source operating within the optimal frequency range), and 3.5 GHz (increased power dissipation due to high attenuation).